






RESEARCH ARTICLE | JULY 20 2023

# Molecular semiconductors and the Ioffe–Regel criterion: A terahertz study on band transport in DBTTT

P. Riederer ; F. Devaux; G. Schweicher ; Y. H. Geerts ; R. Kersting  




*Appl. Phys. Lett.* 123, 032103 (2023)

<https://doi.org/10.1063/5.0153710>

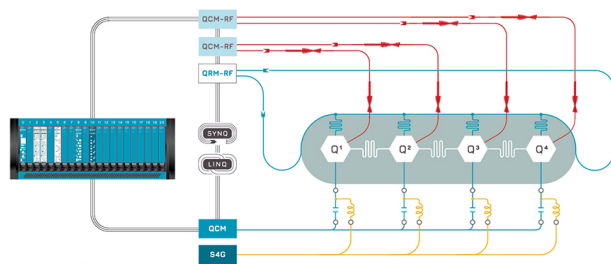


CrossMark

 QBLOX

Integrates all Instrumentation + Software for Control and Readout of

**Superconducting Qubits**  
**NV-Centers**  
**Spin Qubits**



Superconducting Qubit Setup

[find out more >](#)

# Molecular semiconductors and the Ioffe–Regel criterion: A terahertz study on band transport in DBTTT

Cite as: Appl. Phys. Lett. **123**, 032103 (2023); doi: [10.1063/5.0153710](https://doi.org/10.1063/5.0153710)

Submitted: 11 April 2023 · Accepted: 30 June 2023 ·

Published Online: 20 July 2023



View Online



Export Citation



CrossMark

P. Riederer,<sup>1</sup>  F. Devaux,<sup>2</sup> G. Schweicher,<sup>2</sup>  Y. H. Geerts,<sup>2</sup>  and R. Kersting<sup>1,a)</sup> 

## AFFILIATIONS

<sup>1</sup>Photonics and Optoelectronics Group, Faculty of Physics and Center for NanoScience (CeNS), Ludwig-Maximilians-Universität, Königinstr. 10, 80539 München, Germany

<sup>2</sup>Laboratoire de chimie des polymères, Faculté des Sciences, Université Libre de Bruxelles, ULB Boulevard du Triomphe, Brussels 1050, Belgium

<sup>a)</sup>Author to whom correspondence should be addressed: [roland.kersting@lmu.de](mailto:roland.kersting@lmu.de)

## ABSTRACT

Terahertz electromodulation spectroscopy provides insight into the physics of charge carrier transport in molecular semiconductors. The work focuses on thin-film devices of dibenzothiopheno[6,5-b:6',5'-f]thieno[3,2-b]thiophene. Frequency-resolved data show a Drude-like response of the hole gas in the accumulation region. The temperature dependence of the mobilities follows a  $T^{1/2}$  power law. This indicates that the thermal mean free path of the charge carriers is restricted by disorder. Only a fraction of approximately 5% of the injected carriers fulfills the Ioffe–Regel criterion and participates in band transport.

© 2023 Author(s). All article content, except where otherwise noted, is licensed under a Creative Commons Attribution (CC BY) license (<http://creativecommons.org/licenses/by/4.0/>). <https://doi.org/10.1063/5.0153710>

Several factors limit the charge carrier transport in the accumulation region of organic field-effect devices. These can be intrinsic material properties, such as small orbital overlap between semiconductor molecules or phonon scattering, and extrinsic factors, such as impurities or the dielectric roughness at the interface to the gate insulator. Studies on field-effect transistors (FETs) have shown that the interface roughness due to static disorder strongly reduces mobility.<sup>1–3</sup> Furthermore, random dipole fields within the channel region scatter charge carriers.<sup>4,5</sup> Structural disorder within the first monolayers may also limit transport.<sup>6,7</sup>

Temperature-resolved measurements of the mobility  $\mu$  help to identify the dominant scattering mechanisms by their characteristic temperature dependencies, for instance,  $\mu \sim T^{3/2}$  for scattering at ions and  $\mu \sim T^{-3/2}$  for phonon scattering. Terahertz electromodulation spectroscopy facilitates temperature-resolved studies of charge transport in organic semiconductors.<sup>8</sup> The technique provides access to band transport, but is insensitive to slow transport processes, such as hopping. In this work, we present a terahertz (THz) study on field-effect devices made of dibenzothiopheno[6,5-b:6',5'-f]thieno[3,2-b]thiophene (DBTTT).<sup>9</sup> Hole mobilities of up to  $\mu = 3 \text{ cm}^2/\text{Vs}$  are found. Frequency-resolved data indicate that the band transport of the carriers is limited by disorder in the accumulation region. This is

consistent with the temperature dependence of the mobility, which follows  $\mu \sim T^{1/2}$ . The results show that most charge carriers do not participate in band transport. Their mean free paths do not satisfy the Ioffe–Regel criterion.

Figure 1(a) illustrates the conceptual outline of THz electromodulation spectroscopy. Few-cycle THz pulses are transmitted through field-effect devices that comprise an injection layer, a semiconductor thin film, an insulator, and a gate contact. With the application of a gate voltage  $V_g$ , charge carriers are injected into the device and accumulate at the interface between the semiconductor and the insulator. In the case of DBTTT, only holes can be injected. They respond to the AC field of the THz pulses and cause absorption and dispersion of the transmitted radiation. Switching the applied voltage  $V_g$  yields a differential transmission signal  $\Delta S$ , which provides the charge carriers' sheet conductance  $\sigma_{2D}$  and mobility  $\mu$ .<sup>8</sup>

Field-effect structures, as illustrated in Fig. 1(b), are fabricated on 0.5 mm-thick sapphire dies and on 125  $\mu\text{m}$ -thick foils of polyethylene naphthalate (PEN). Devices on PEN are advantageous, because its small index of refraction supports the transmission of THz radiation. Temperature-resolved experiments require good heat conduction and are performed on devices with sapphire substrates.

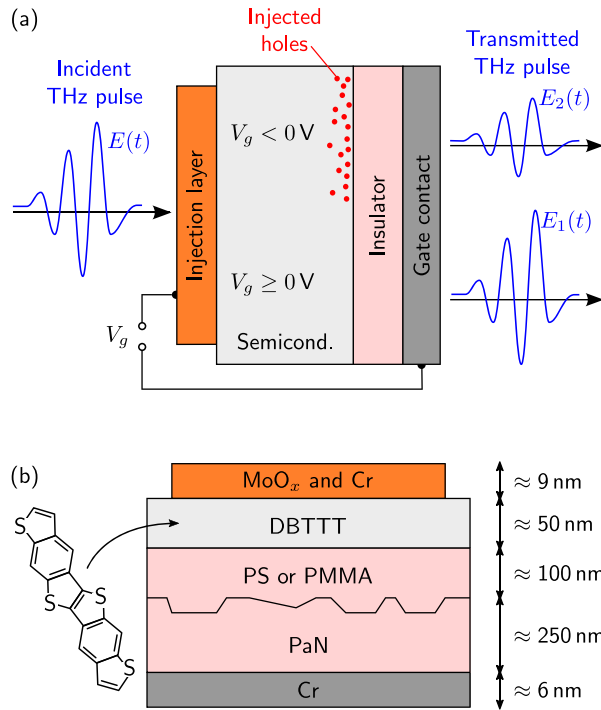


FIG. 1. Illustration of the method of THz electro-modulation spectroscopy (a). Schematic device architecture (b).

The devices' injection contacts consist of MoO<sub>x</sub> and Cr, and the gate contacts are made of Cr. Typical thicknesses of the layers are between 6 and 9 nm, which permits the sufficient transmission of THz radiation. The insulator parylene N (PaN) is deposited by chemical vapor deposition. Pinhole-free films are obtained for thicknesses exceeding 250 nm. These films, however, have an RMS roughness of approximately 5 nm, which leads to an inhomogeneous growth of DBTTT when deposited on top (supplementary material, Figs. S1 and S3). Therefore, the PaN is planarized by spin coating of polystyrene (PS) or poly(methyl methacrylate) (PMMA). The PS and PMMA have average molecular weights of 10 and 950 kDa, respectively. A 1.5 wt. % solution in toluene for the PS film and a 2 wt. % solution in dichlorobenzene for the PMMA are used. The solutions are spin coated at 3000 rpm onto the PaN and then dried at 140 °C for 2 h. The thickness of the planarization layers is approximately 50 nm. Planarization with PS and with PMMA reduces the RMS roughness of the gate insulator to 1.2 nm. The chromium gate contact, the injection layer, and the DBTTT are deposited by physical vapor deposition at  $p \approx 5 \times 10^{-7}$  mbar, with deposition rates of approximately 0.1 Å/s. All DBTTT films are polycrystalline and have a thickness of approximately 50 nm. The devices have active areas of 28 mm<sup>2</sup> and unit capacitances of  $\tilde{C} \approx 7.2$  nF/cm<sup>2</sup>.

Terahertz electromodulation experiments are performed with few-cycle THz pulses that have a bandwidth of 2.6 THz. The details of the experimental setup can be found in Ref. 8. Figure 2 shows the relative differential transmission  $\Delta S/S$  of THz radiation during the modulation of the applied voltage  $V_g$ . The data are recorded at the temporal peak of the THz pulse (see Fig. 3). Figure 2 shows that at  $V_g < 0$ , holes

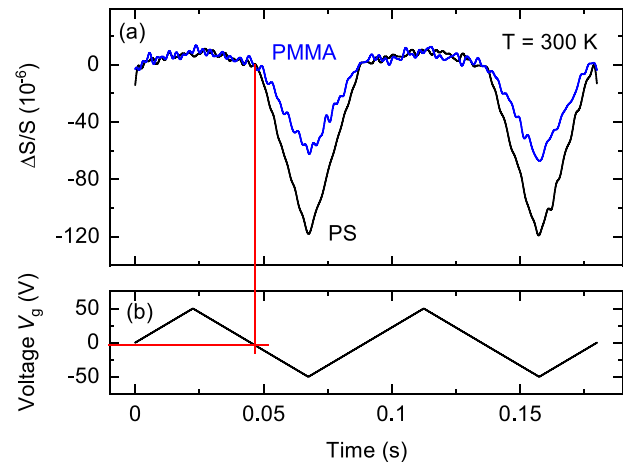


FIG. 2. Dependence of the relative differential THz signal  $\Delta S/S$  on the modulation voltage  $V_g$  recorded at  $T = 300$  K. Data obtained on structures with a PMMA interlayer and a PS interlayer are shown in (a) by blue and black lines, respectively. Applied modulation voltage  $V_g$  between bottom and top contact (b). The red lines indicate that the threshold voltage  $V_{th}$  is marginal.

are injected into the DBTTT and accumulate at the interface to the insulator. Their response to the THz field reduces the transmission signal by  $\Delta S$ . An injection of mobile electrons at  $V_g > 0$  is not observed.

The sheet conductance of the injected charge carriers can be obtained from the data in Fig. 2 using an equivalent of Tinkham's formula:<sup>10,11</sup>

$$\sigma_{2D} = e \mu n_{2D} = -\frac{\Delta S}{S} \cdot \frac{2\sqrt{\epsilon_b}}{Z_0}, \quad (1)$$

where  $\epsilon_b$  is the relative permittivity of the layer,  $Z_0$  is the impedance of free space,  $e$  is the elementary charge, and  $n_{2D}$  is the modulated two-dimensional charge carrier density. The sheet density of injected holes  $n_{2D,inj}$  is calculated from  $V_g$  and  $\tilde{C}$ . For example, a gate voltage of  $V_g = -50$  V leads to  $n_{2D,inj} \approx 2.2 \times 10^{12}$  cm<sup>-2</sup>. Assuming that all injected holes are mobile, their mobility is given by  $\mu_{inj} = \sigma_{2D}/(en_{2D,inj})$ , which provides  $\mu_{inj} = 3.0$  cm<sup>2</sup>/V s for devices planarized

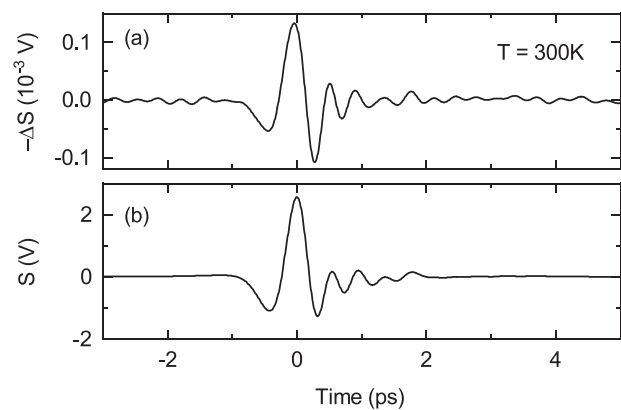


FIG. 3. Time-resolved THz transmission through DBTTT on PS. (a) Differential signal  $\Delta S$  due to the injection of holes. (b) Transmitted THz signal  $S$ .

with PS and  $\mu_{inj} = 1.5 \text{ cm}^2/\text{V s}$  for the ones planarized with PMMA. Similar values have been reported for DBTTT FETs.<sup>9</sup>

Although the PS layer and the PMMA layer have similar surface roughness, the measured mobilities differ by a factor of 2. This observation agrees with previous works,<sup>4,5,12</sup> wherein it is attributed to the different dielectric properties of PS and PMMA, which have relative permittivities of  $\epsilon = 2.6$  and  $\epsilon = 3.0$ , respectively. An increased permittivity reduces the mobility,<sup>4,5</sup> presumably because random dipoles within the insulator broaden the semiconductors' density of states at the interface. A recent study concludes that the polarity of the insulator reduces the mobility.<sup>12</sup> The mobilities for PS and PMMA surfaces reported in Ref. 12 show nearly the same ratio as the values obtained from the data in Fig. 2.

Despite the agreement with the above works, one fundamental question has not been addressed: Are all of the injected charge carriers mobile and contribute to band transport? If only a part of the injected carriers were mobile ( $n_{2D,mob} < n_{2D,inj}$ ), the mobility of these carriers increases according to  $\mu_{mob} = \sigma_{2D}/(e n_{2D,mob})$ . Insight is gained by analyzing the frequency dependence of the carriers' AC conductivity, for which we assume band transport, because typical hopping conductivities are too small to be observed in our THz experiments. Various transport models have been applied for interpreting the THz response of charge carriers in organic semiconductors, among which are the fundamental Drude model,<sup>13,14</sup> the Drude–Smith model,<sup>15,16</sup> the localization-modified Drude model,<sup>17–19</sup> and the Drude–Anderson model.<sup>20–22</sup> A brief discussion of the applicability of these models is given in the supplementary material. Only the classical Drude model fulfills the requirements and provides a reasonable agreement with the experimental data, as shown by Fig. S9 of the supplementary material. Thus, we use this model as the most reasonable approach for describing charge transport.

For a Drude response with momentum relaxation time  $\tau$ , the sheet conductivity is as follows:

$$\sigma_{2D}(\omega) = \frac{n_{2D} e^2 \tau}{m_h^*} \cdot \frac{1 + i \omega \tau}{1 + \omega^2 \tau^2}. \quad (2)$$

Terahertz spectroscopy can resolve this frequency dependence by recording transmission changes in the time domain, followed by Fourier transformation.<sup>23</sup> Figure 3 shows time-resolved transmission data recorded at room temperature. The differential signal  $\Delta S$  is obtained by square-wave modulation with  $V_g = \pm 50 \text{ V}$  at frequencies of approximately 10 Hz. Compared to the transmitted signal  $S$ , the transmission change  $\Delta S$  is minute, which illustrates the weak interaction between THz radiation and the mobile holes.

Fourier transforms of the experimental data of  $\Delta S/S$  are shown in Fig. 4 by the symbols. The solid lines in Fig. 4 are fits to the experimental data and consider a Drude response, as described in Eq. (2). The same parameter sets of Drude scattering time  $\tau$  and sheet density  $n_{2D}$  are used for both the real part and the imaginary part of  $\Delta S/S$ . For the hole's effective mass,  $m_h^* = m_e$  is used.<sup>24</sup> A description of the analysis of  $\Delta S/S$  can be found in the supplementary material or in Ref. 8. The carrier mobilities are deduced from the fit parameter  $\tau$  using  $\mu = e \tau / m_h^*$ .

A reasonable agreement between experimental data and calculations can only be achieved if a strongly reduced density of mobile carriers is assumed (compared to Fig. S8 of the supplementary material). The solid lines in Fig. 4 show calculations for  $n_{2D,mob} = 0.05 \cdot n_{2D,inj}$ .

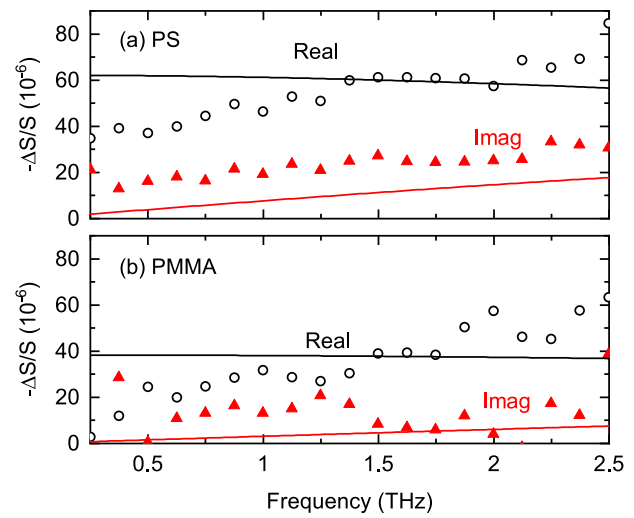
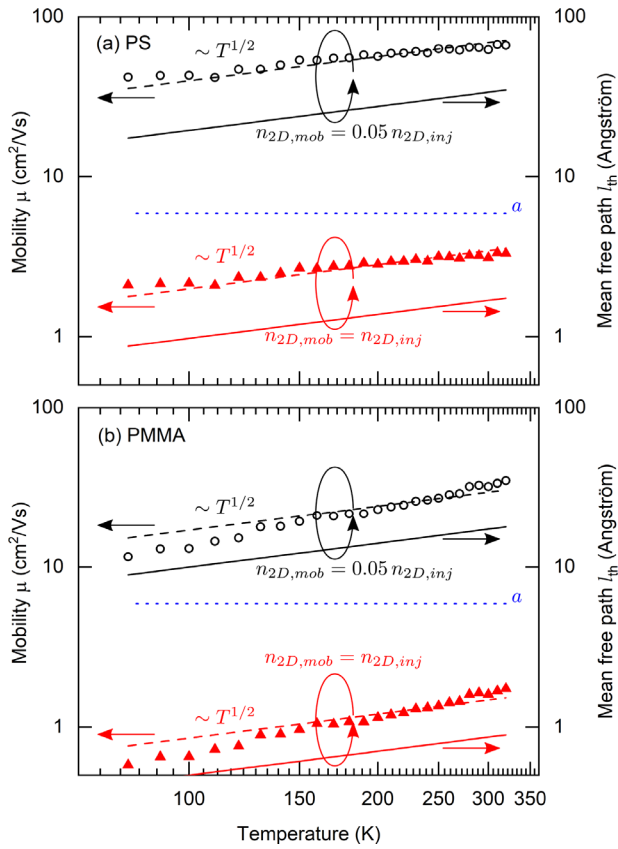


FIG. 4. Frequency dependence of the relative differential transmission  $\Delta S/S$  for DBTTT on PS (a) and for DBTTT on PMMA (b) recorded at  $T = 300 \text{ K}$ . The real and imaginary parts of  $\Delta S/S$  are depicted by black circles and by red triangles, respectively. Fits to the experimental data are shown by black lines and red lines for the real and imaginary parts, respectively.

Under this assumption, Drude mobilities for this fraction of charge carriers of  $\mu = 35$  and  $\mu = 23 \text{ cm}^2/\text{V s}$  are deduced for the devices planarized with PS and PMMA, respectively. For these extrapolations, the same fraction of 5% is assumed for PS and PMMA. The value of 5% has large error margins, and more precise values are unreasonable. However, the findings indicate that charge transport mainly results from a small fraction of the injected charge carriers, whereas most carriers have no significant contribution to transport. They may be trapped or perform hopping transport, both of which are not accessible in THz experiments. A recent work considers the Boltzmann transport equation in conjunction with the most dominating scattering process and concludes that even mobile carriers may be immobilized by strong scattering.<sup>25</sup> The authors discuss a transport reduction factor, which may be related to our observation that only a small fraction of the charge carriers participates in transport.

Temperature-resolved measurements support the framework that only a fraction of charge carriers participates in band transport. The experimental data in Fig. 5 are obtained by recording  $\Delta S/S$  at the temporal peak of the THz pulse and by modulating the device with a square wave of  $V_g = \pm 50 \text{ V}$ . The observed temperature dependencies result from the THz response of the injected holes and not from the temperature dependence of the injection process: The slopes of the transmission changes in Fig. 2 are linear, even at low temperatures. This indicates that the transfer across the injection interface is faster than the modulation and does not cause the temperature dependencies in Fig. 5. Measurements in the dependence of the modulation frequency confirm this.

The mobilities shown in Fig. 5 are deduced for two cases: (i) by assuming that all injected carriers contribute to the THz signal (red triangles) and (ii) by considering that only a fraction  $n_{2D,mob} \approx 0.05 \cdot n_{2D,inj}$  of the injected carriers is mobile (black circles). The dashed red and black lines are fits that follow the power law  $\mu \sim T^{1/2}$ . Both the



**FIG. 5.** Temperature dependence of the mobilities in DBTTT deposited on PS (a) and PMMA (b). Mobilities are obtained from  $\Delta S/S$  by assuming either  $n_{2D,mob} = n_{2D,inj}$  or  $n_{2D,mob} = 0.05 \cdot n_{2D,inj}$  and are displayed by red triangles and black circles, respectively. The dashed lines follow  $\mu \sim T^{1/2}$  and serve as visual guides. The solid lines show the temperature dependence of the thermal mean free path  $\ell_{th}$  for the above densities. The blue dotted line indicates the size of the unit cell  $a$ .

mobilities obtained on the PS structures and on those of PMMA structures follow this dependence. This behavior clearly distinguishes from the dependence of  $T^{-1/2}$  or  $T^{-3/2}$ , which is expected for dynamic localization and phonon scattering, respectively.<sup>26</sup>

The observed  $T^{1/2}$  power law of the mobilities can be explained by a reduced mean free path of the charge carriers due to disorder. According to the Ioffe–Regel criterion, extended Bloch waves can only exist if the carriers’ thermal mean free path  $\ell_{th}$  exceeds the size of the unit cell  $a$ .<sup>27,28</sup> In an accumulation layer with areas of different degrees of disorder, only regions with  $\ell_{th} > a$  support band transport. Only here, charge carriers can exhibit a Drude response. In regions where  $\ell_{th}$  does not fulfill the Ioffe–Regel criterion, charge carrier transport is limited to hopping. Thus, THz experiments access only those regions where charge carriers have sufficient mean free path. However, even in these high-mobility regions, diagonal disorder increases the width of the density of states,<sup>4</sup> which in turn partially limits the carrier’s mean free path.

Disorder is unintentionally introduced during the deposition of the molecular semiconductor or may result from the interface

roughness of the insulator<sup>3,29</sup> or from its dielectric disorder.<sup>4</sup> Independent of the origin of disorder, it limits the thermal mean free path  $\ell_{th} = v_{th}\tau$ , which can be expressed by the mobility as

$$\ell_{th} = \frac{\mu}{e} \sqrt{2 k_B T m_h^*}, \quad (3)$$

when assuming a two-dimensional carrier gas at the interface to the insulator. The experimental mobility data and the calculations of the mean free paths in Fig. 5 follow the same temperature dependence  $T^{1/2}$ . This indicates that properties of the mean free path control the observed mobility.

The calculations of the mean free path  $\ell_{th}$  in Fig. 5 are based on the room-temperature mobilities of the devices and on the extrapolation of the temperature dependence according to Eq. (3). Two cases are considered: (i) that all injected charge carriers are mobile (red solid lines) and (ii) that  $n_{2D,mob} = 0.05 \cdot n_{2D,inj}$  (black solid lines). Furthermore, the dotted blue lines indicate the lattice constant  $a = 5.91 \text{ \AA}$  of DBTTT.<sup>30</sup> For both of the investigated structures,  $\ell_{th} < a$  when considering for the mobile carrier density  $n_{2D,mob} = n_{2D,inj}$ . This, however, would not fulfill the Ioffe–Regel criterion, and a THz signature of the charge carriers would not be observable, which contradicts the experimental results, such as in Figs. 2–4. One option to resolve this contradiction is to assume a spatially inhomogeneous semiconductor, comprised of regions where  $\ell_{th} > a$  as well as of regions with  $\ell_{th} < a$ . Thus, only a part of the injected carriers exhibit band transport and contribute to the THz signal, for which classical Drude transport can be assumed. The others perform hopping transport and are not detected in the THz experiments. The calculations of Fig. 5 show that  $\ell_{th}$  exceeds the lattice constant when assuming that only 5% of the charge carriers contribute to the mobility. Only these 5% fulfill the Ioffe–Regel criterion and participate in band transport. The density of interface defects, which localize charge carriers, can spread over a wide range, and even for single crystals, values between  $0.7 \times 10^{10}$  and  $2 \times 10^{12} \text{ cm}^{-2}$  have been reported.<sup>31,32</sup> Thus, the observation that only 5% of the charge carriers participate in band transport is plausible.

Altogether, the result that only a fraction of the injected charge carriers participates in band transport is derived from the following observations: (i) the spectral response of the charge carriers (Fig. 4). The agreement between the experimental data and calculation requires that  $n_{2D,mob} < n_{2D,inj}$ . (ii) The temperature dependence of the mobilities follows a  $T^{1/2}$  power law (Fig. 5). This shows that the dominating scattering process is not phonon scattering, for which  $\mu \sim T^{-3/2}$  is expected. Also, the dynamic localization can be excluded, for which temperature dependencies between  $\mu \sim T^{-3/2}$  and  $\mu \sim T^{-1/2}$  are expected.<sup>26</sup> This leaves disorder scattering as the most potential process that limits the mobility. Disorder scattering may arise because of structural disorder of the semiconductor<sup>1–3</sup> and because of local fields within the insulator.<sup>4,5</sup> In areas where potential fluctuations occur on the scale of few unit cells, disorder leads to localization and reduces the fraction of mobile carriers that perform band transport. (iii) The result is that the mean free paths do not exceed the size of the unit cell when assuming that all carriers contribute to band transport (Fig. 5). In this case, the Ioffe–Regel criterion would not be fulfilled and band transport would be impossible. Overall agreement with the experimental data can be achieved under

the assumption that only a fraction of the injected carriers participates in band transport.

The result that disorder excludes most of the injected carriers from band transport underpins the technological importance of improving the interfacial properties between insulator and semiconductor. High-mobility devices of molecular thin films may require surface engineering of the interface, such as by the functionalization and planarizing of the insulating layer,<sup>33,34</sup> the use of self-assembled monolayers,<sup>35,36</sup> or the fabrication of semiconductor heterostructures.<sup>37–39</sup>

In summary, we investigated charge transport in DBTTT field-effect devices utilizing THz electromodulation spectroscopy. Mobilities of 3.0 and 1.5 cm<sup>2</sup>/V s are found for DBTTT deposited on PS and PMMA, respectively, assuming that all injected charge carriers contribute to band transport. However, frequency-resolved data and temperature-resolved data indicate that only a fraction of the injected charge carriers participates in band transport. The vast majority is either trapped or performs hopping transport. Their mean free paths are smaller than the semiconductor's unit cell, which violates the Ioffe–Regel criterion and excludes them from band transport. Mobility estimates for the fraction of carriers that fulfill the Ioffe–Regel criterion lead to values above 20 cm<sup>2</sup>/V s.

See the supplementary material for details on the device architecture, thin-film topographies, data analysis, and other transport models.

This research was funded by the Deutsche Forschungsgemeinschaft (DFG, German Research Foundation) (Contract No. KE 516/11-1). G.S. thanks the Belgian National Fund for Scientific Research (FNRS) for financial support through research project COHERENCE2 no. F.4536.23. G.S. is a FNRS Research Associate. G.S. acknowledges the financial support from the Francqui Foundation (Francqui Start-Up Grant). Y.G. is thankful to FNRS for financial support through research projects Pi–Fast (No. T.0072.18) and Pi–Chir (No. T.0094.22).

## AUTHOR DECLARATIONS

### Conflict of Interest

The authors have no conflicts to disclose.

### Author Contributions

**Philipp Riederer:** Data curation (equal); Formal analysis (equal); Validation (equal); Visualization (equal); Writing – original draft (equal); Writing – review & editing (equal). **Félix Devaux:** Resources (lead). **Guillaume Schweicher:** Project administration (equal); Writing – review & editing (supporting). **Yves H. Geerts:** Conceptualization (equal); Project administration (equal); Supervision (equal); Writing – review & editing (supporting). **Roland Kersting:** Conceptualization (equal); Formal analysis (equal); Project administration (equal); Supervision (equal); Writing – original draft (equal); Writing – review & editing (equal).

### DATA AVAILABILITY

The data that support the findings of this study are available from the corresponding author upon reasonable request.

## REFERENCES

- Studel, S. D. Vusser, S. D. Jonge, D. Janssen, S. Verlaak, J. Genoe, and P. Heremans, "Influence of the dielectric roughness on the performance of pentacene transistors," *Appl. Phys. Lett.* **85**, 4400 (2004).
- G. Lin, Q. Wang, L. Peng, M. Wang, H. Lu, G. Zhang, G. Lv, and L. Qiu, "Impact of the lateral length scales of dielectric roughness on pentacene organic field-effect transistors," *J. Phys. D: Appl. Phys.* **48**, 105103 (2015).
- M. Geiger, R. Acharya, E. Reutter, T. Ferschke, U. Zschieschang, J. Weis, J. Pflaum, H. Klauk, and R. T. Weitz, "Effect of the degree of the gate-dielectric surface roughness on the performance of bottom-gate organic thin-film transistors," *Adv. Mater. Interfaces* **7**, 1902145 (2020).
- J. Veres, S. D. Ogier, S. W. Leeming, D. C. Cupertino, and S. M. Khaffaf, "Low-k insulators as the choice of dielectrics in organic field effect transistors," *Adv. Funct. Mater.* **13**, 199 (2003).
- A. F. Stassen, R. W. I. de Boer, N. N. Iosad, and A. F. Morpurgo, "Influence of the gate dielectric on the mobility of rubrene single-crystal field-effect transistors," *Appl. Phys. Lett.* **85**, 3899 (2004).
- X. Sun, C. Di, and Y. Liu, "Engineering of the dielectric-semiconductor interface in organic field-effect transistors," *J. Mater. Chem.* **20**, 2599 (2010).
- Y. D. Park, J. A. Lim, H. S. Lee, and K. Cho, "Interface engineering in organic transistors," *Mater. Today* **10**, 46 (2007).
- P. Riederer and R. Kersting, "Terahertz electromodulation spectroscopy for characterizing electronic transport in organic semiconductor thin films," *J. Infrared Millim. THz Waves* **44**, 1–16 (2023).
- J.-I. Park, J. W. Chung, J.-Y. Kim, J. Lee, J. Y. Jung, B. Koo, B.-L. Lee, S. W. Lee, Y. W. Jin, and S. Y. Lee, "Dibenzothiopheno [6,5-b:6',5'-f]thieno [3,2-b]thiophene (dbttt): High-performance small-molecule organic semiconductor for field-effect transistors," *J. Am. Chem. Soc.* **137**, 12175 (2015).
- R. E. Glover and M. Tinkham, "Conductivity of superconducting films for photon energies between 0.3 and 40kt," *Phys. Rev.* **108**, 243 (1957).
- S. Funk, G. Acuna, M. Handloser, and R. Kersting, "Probing the momentum relaxation time of charge carriers in ultrathin layers with terahertz radiation," *Opt. Express* **17**, 17450 (2009).
- T. K. Rockson, S. Baek, H. Jang, S. Oh, G. Choi, H. H. Choi, and H. S. Le, "Macroscopic interfacial property as a determining parameter for reliable prediction of charge mobility in organic transistors," *J. Phys. Chem. C* **122**, 17695 (2018).
- M. Fischer, M. Dressel, B. Gompf, A. K. Tripathi, and J. Pflaum, "Infrared spectroscopy on the charge accumulation layer in rubrene single crystals," *Appl. Phys. Lett.* **89**, 182103 (2006).
- R. Uchida, H. Yada, M. Makino, Y. Matsui, K. Miwa, T. Uemura, J. Takeya, and H. Okamoto, "Charge modulation infrared spectroscopy of rubrene single-crystal field-effect transistors," *Appl. Phys. Lett.* **102**, 093301 (2013).
- N. V. Smith, "Classical generalization of the Drude formula for the optical conductivity," *Phys. Rev. B* **64**, 155106 (2001).
- H. Yada, H. Sekine, T. Miyamoto, T. Terashige, R. Uchida, T. Otaki, F. Maruike, N. Kida, T. Uemura, S. Watanabe, T. Okamoto, J. Takeya, and H. Okamoto, "Evaluating intrinsic mobility from transient terahertz conductivity spectra of microcrystal samples of organic molecular semiconductors," *Appl. Phys. Lett.* **115**, 143301 (2019).
- K. Lee, A. J. Heeger, and Y. Cao, "Reflectance of polyaniline protonated with camphor sulfonic acid: Disordered metal on the metal-insulator boundary," *Phys. Rev. B* **48**, 14884 (1993).
- Z. Q. Li, V. Podzorov, N. Sai, M. C. Martin, M. E. Gershenson, M. D. Ventra, and D. N. Basov, "Light quasiparticles dominate electronic transport in molecular crystal field-effect transistors," *Phys. Rev. Lett.* **99**, 016403 (2007).
- M. Yamashita, C. Otani, M. Shimizu, and H. Okuzaki, "Effect of solvent on carrier transport in poly(3,4-ethylenedioxythiophene)/poly(4-styrenesulfonate) studied by terahertz and infrared-ultraviolet spectroscopy," *Appl. Phys. Lett.* **99**, 143307 (2011).
- S. Fratini, S. Ciuchi, and D. Mayou, "Phenomenological model for charge dynamics and optical response of disordered systems: Application to organic semiconductors," *Phys. Rev. B* **89**, 235201 (2014).
- H. Yada, R. Uchida, H. Sekine, T. Terashige, S. Tao, Y. Matsui, N. Kida, S. Fratini, S. Ciuchi, Y. Okada, T. Uemura, J. Takeya, and H. Okamoto, "Carrier dynamics of rubrene single-crystals revealed by transient broadband terahertz spectroscopy," *Appl. Phys. Lett.* **105**, 143302 (2014).

- <sup>22</sup>Y. Han, T. Miyamoto, T. Otaki, N. Takamura, N. Kida, N. Osakabe, J. Tsurumi, S. Watanabe, T. Okamoto, J. Takeya, and H. Okamoto, "Scattering mechanism of hole carriers in organic molecular semiconductors deduced from analyses of terahertz absorption spectra using Drude-Anderson model," *Appl. Phys. Lett.* **120**, 053302 (2022).
- <sup>23</sup>T. R. Arend, A. Wimmer, G. Schweicher, B. Chattopadhyay, Y. H. Geerts, and R. Kersting, "Band transport and trapping in didodecyl [1]benzothieno [3,2-b] [1]benzothiophene probed by terahertz spectroscopy," *J. Phys. Chem. Lett.* **8**, 5444 (2017).
- <sup>24</sup>M. Ohtomo, T. Suzuki, T. Shimada, and T. Hasegawa, "Band dispersion of quasi-single crystal thin film phase pentacene monolayer studied by angle-resolved photoelectron spectroscopy," *Appl. Phys. Lett.* **95**, 123308 (2009).
- <sup>25</sup>X. Wang, L. F. Register, and A. Dodabalapur, "Redefining the mobility edge in thin-film transistors," *Phys. Rev. Appl.* **11**, 064039 (2019).
- <sup>26</sup>S. Fratini and S. Ciuchi, "Bandlike motion and mobility saturation in organic molecular semiconductors," *Phys. Rev. Lett.* **103**, 266601 (2009).
- <sup>27</sup>N. F. Mott and E. A. Davis, *Electronic Processes in Non-Crystalline Materials* (Clarendon Press, 1979).
- <sup>28</sup>N. F. Mott and M. Kaveh, "Metal-insulator transitions in non-crystalline systems," *Adv. Phys.* **34**, 329 (1985).
- <sup>29</sup>P. Riederer, M. Bouraoui, and R. Kersting, "Impact of surface roughness on conduction in molecular semiconductors," *Appl. Phys. Lett.* **120**, 112103 (2022).
- <sup>30</sup>E.-K. Lee, M. Y. Lee, A. Choi, J.-Y. Kim, O. Y. Kweon, J.-H. Kim, J. Y. Jung, T.-J. Shin, J. H. Oh, J.-I. Park, and S. Y. Lee, "Phenyl derivative of dibenzothiopheno [6,5-b:6',5'-f]-thieno [3,2-b]thiophene (DPh-DBTTT): High thermally durable organic semiconductor for high-performance organic field-effect transistors," *Adv. Electron. Mater.* **3**, 1700142 (2017).
- <sup>31</sup>V. Podzorov, E. Menard, A. Borissov, V. Kiryukhin, J. A. Rogers, and M. E. Gershenson, "Intrinsic charge transport on the surface of organic semiconductors," *Phys. Rev. Lett.* **93**, 86602 (2004).
- <sup>32</sup>C. Goldmann, C. Krellner, K. P. Pernstich, S. Haas, D. J. Gundlach, and B. Batlogg, "Determination of the interface trap density of rubrene single-crystal field-effect transistors and comparison to the bulk trap density," *J. Appl. Phys.* **99**, 034507 (2006).
- <sup>33</sup>T. Yokota, T. Kajitani, R. Shidachi, T. Tokuhara, M. Kaltenbrunner, Y. Shoji, F. Ishiwari, T. Sekitani, T. Fukushima, and T. Someya, "A few-layer molecular film on polymer substrates to enhance the performance of organic devices," *Nat. Nanotechnol.* **13**, 139 (2018).
- <sup>34</sup>M. Sugiyama, S. Jancke, T. Uemura, M. Kondo, Y. Inoue, N. Namba, T. Araki, T. Fukushima, and T. Sekitani, "Mobility enhancement of DNTT and BTBT derivative organic thin-film transistors by triptycene molecule modification," *Org. Electron.* **96**, 106219 (2021).
- <sup>35</sup>R. Acharya, B. Peng, P. K. L. Chan, G. Schmitz, and H. Klauk, "Achieving ultralow turn-on voltages in organic thin-film transistors: Investigating fluoroalkylphosphonic acid self-assembled monolayer hybrid dielectrics," *Appl. Mater. Interfaces* **11**, 27104 (2019).
- <sup>36</sup>M. Geiger, L. Schwarz, U. Zschieschang, D. Manske, J. Pflaum, J. Weis, H. Klauk, and R. T. Weitz, "Quantitative analysis of the density of trap states in semiconductors by electrical transport measurements on low-voltage field-effect transistors," *Phys. Rev. Appl.* **10**, 044023 (2018).
- <sup>37</sup>X. Qian, T. Wang, and D. Yan, "High mobility organic thin-film transistors based on p-p heterojunction buffer layer," *Appl. Phys. Lett.* **103**, 173512 (2013).
- <sup>38</sup>O. D. Jurchescu, M. Popinciuc, B. J. van Wees, and T. T. M. Palstra, "Interface-controlled, high-mobility organic transistors," *Adv. Mater.* **19**, 688 (2007).
- <sup>39</sup>A. Choi, Y.-N. Kwon, J. W. Chung, Y. Yun, J.-I. Park, and Y. U. Lee, "Control of dielectric surface energy by dry surface treatment for high performance organic thin film transistor based on dibenzothiopheno [6,5-b:6',5'-f] thieno [3,2-b] thiophene semiconductor," *AIP Adv.* **10**, 025127 (2020).